

Analytical Solution for the Displacement Field in Composite Single-Lap Shear Joints With Zero-Thickness Interfaces

Schiller, A.; Castro, Saullo G.P.; Bisagni, C.

DOI

10.2514/6.2025-2338

Publication date

2025

Document Version

Final published version

Published in

Proceedings of the AIAA SCITECH 2025 Forum

Citation (APA)

Schiller, A., Castro, S. G. P., & Bisagni, C. (2025). Analytical Solution for the Displacement Field in Composite Single-Lap Shear Joints With Zero-Thickness Interfaces. In *Proceedings of the AIAA SCITECH 2025 Forum* Article AIAA 2025-2338 (AIAA Science and Technology Forum and Exposition, AIAA SciTech Forum 2025). https://doi.org/10.2514/6.2025-2338

Important note

To cite this publication, please use the final published version (if applicable).

Please check the document version above.

Copyright

Other than for strictly personal use, it is not permitted to download, forward or distribute the text or part of it, without the consent of the author(s) and/or copyright holder(s), unless the work is under an open content license such as Creative Commons.

Takedown policy

Please contact us and provide details if you believe this document breaches copyrights.

We will remove access to the work immediately and investigate your claim.



Analytical Solution for the Displacement Field in Composite Single-Lap Shear Joints with Zero-Thickness Interfaces

A. Schiller* and S.G.P. Castro[†]

Delft University of Technology, Delft, 2629 HS, Netherlands

C. Bisagni[‡] Politecnico di Milano, Milan, 20156, Italy

An analytical model for predicting the displacement field in composite single-lap shear joints with zero-thickness interfaces is developed and verified with numerical simulations. This two-dimensional model imposes no restrictions on the composite layup or the dimensions of the adherends. It closely aligns with the displacement field predicted by numerical simulations, provided that the assumptions of small deformations and plane strain are satisfied. Small discrepancies are observed near the overlap region because the stress-free boundary condition at the overlap ends is not satisfied exactly. Consequently, the joint stiffness is slightly overestimated compared to the numerical simulations. Nonetheless, the analytical model can serve as a useful tool for providing input for more detailed analyses of single-lap shear joints, for example for determining the interlaminar stress field at the interface between the two adherends.

I. Nomenclature

 A_{ij}, B_{ij}, D_{ij} = extensional, coupling, and bending laminate stiffness matrix elements

A, B, D = laminate stiffness matrices

 $A^{\text{off}}, B^{\text{off}}, D^{\text{off}}$ = laminate stiffness matrices offset to the reference plane

 c_{ii} = undetermined coefficients in the polynomial solution to the eigenvalue problem

C_i = undetermined coefficients in the general solution for the displacement degrees of freedom

C = stiffness matrix

 d_i = distance of region *i* from the reference plane

E = Young's modulus

 E_i Young's modulus in *i*-direction G_{ij} shear modulus in *i j*-direction k shear correction factor l_i length of region i M_{xx} bending stress resultant N_{xx}, N_{xy} in-plane stress resultants Q_x transverse shear stress resultant Q_{ij} ply stiffness matrix elements

R = rotation matrix S = compliance matrix

 \overline{S} = compliance matrix in local ply coordinate system

 t_i = thickness of region i

 u_{init} = prescribed displacement load

 u_i, v_i, w_i = displacements in region i corresponding to the coordinates x_i, y_i , and z_i

 u_{0i}, v_{0i}, w_{0i} = reference plane displacements in region *i*

 x_i, y_i, z_i = Cartesian coordinates in region i

 ε_{ij} = strain tensor components

^{*}Ph.D. Candidate, Aerospace Structures & Materials, A.Schiller@tudelft.nl, AIAA Student Member.

[†]Associate Professor, Aerospace Structures & Materials, S.G.P.Castro@tudelft.nl.

^{*}Professor, Department of Aerospace Science and Technology, Chiara.Bisagni@polimi.it, AIAA Fellow.

 $\varepsilon_{ij}^{(0)}$ = mid-plane contribution to the strain tensor components κ_{ij} = curvature contribution to the strain tensor components λ = eigenvalues, roots of the characteristic equation ν = Poisson's ratio ν = Poisson's ratio in ij-direction ν = stress tensor components ν = rotation of normal to the reference plane about the ν -axis in region ν

II. Introduction

Joints are usually weak points in any type of structure because they exhibit unfavorable loading conditions and sudden changes in stiffness which give rise to stress fields that decrease the load-carrying efficiency of the surrounding material. It is therefore highly relevant to be able to predict the resulting stress distributions, especially in sectors like the aerospace industry where lightweight designs are required to operate safely. Consequently, many tools have been developed to estimate the structural response of joints during preliminary design, in particular for riveted [1, 2] and adhesively bonded [3–6] single-lap shear (SLS) joints.

In recent years, a new pathway has been opened by welded thermoplastic carbon fiber-reinforced polymers (CFRPs). Thermoplastic CFRPs offer several advantages over their thermosetting counterparts, for example improved impact and fracture toughness, 'infinite' shelf life, as well as the potential for recycling [7]. Another benefit is the increased structural efficiency made possible by thermoplastic welding [8]. Compared to adhesive bonding, thermoplastic welding does not require extensive surface treatment which simplifies the manufacturing process. However, previously developed tools and methods for the preliminary design of riveted and adhesively bonded joints are not applicable to thermoplastic welded joints because the corresponding approaches assume the presence of either rivets or an adhesive in the bondline.

An intuitive starting point for creating models for thermoplastic welded joints is building on the ideas from the analysis of adhesively bonded joints. Yet, this strategy fails once a zero-thickness bondline is considered: an infinitely thin bondline leads to infinitely large stresses at the joint interface. Therefore, a useful model must also borrow from the ideas for the analysis of interlaminar stresses in composite structures which can deal with zero-thickness interfaces.

The importance of interlaminar stresses close to free edges in composite structures was first highlighted by Pipes and Pagano [9]. Summaries of other relevant publications on the subject are given in [10] and [11]. In principle, the prediction of interlaminar stresses in composite structures requires solving the equilibrium equations for each ply in three dimensions. However, approximations in two dimensions are often employed because of the mathematical complexity of the problem. The general case of an anisotropic body in two dimensions was solved by Wang and Choi [12] based on the work of Lekhnitskii [13], but is very involved. Ply-based solutions often become unwieldily as the thickness of the laminate increases [14]. The interlaminar stress analysis at a skin-stringer interface by Kassapoglou and DiNicola [15] is geometrically similar to the case of the welded thermoplastic SLS joint. Their model predicts the stress field at the end of one skin-stringer run-out and is valid for cross-ply laminates. However, analytical models for the prediction of the stress and displacement fields in thermoplastic welded SLS joints do not appear to be readily available.

This paper introduces an analytical solution for the displacement field in composite SLS joints with zero-thickness interfaces. No special requirements regarding the dimensions of the adherends or their layups are made. The analysis is verified with numerical simulations. The latter are also used for checking the influence of some of the modeling assumptions on the predictions. Limitations and potential applications of the analytical solution are discussed.

III. Linear Elastic Single-lap Shear Joint Analysis

Consider the welded thermoplastic composite single-lap shear (SLS) joint sketched in Fig. 1.

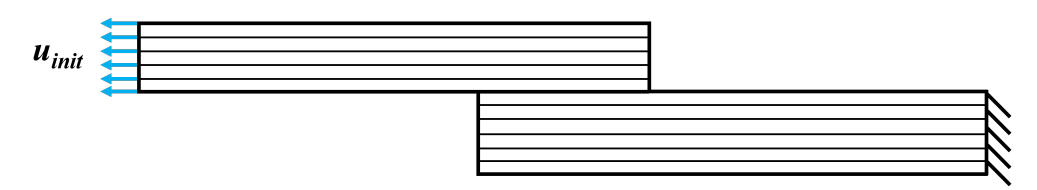


Fig. 1 Welded thermoplastic composite single-lap shear joint subjected to an axial displacement load.

The structure is split into three regions as illustrated in Fig. 2: the upper adherend (U), the lower adherend (L), and the overlap region (O). Each region features a distinct coordinate system at its center. The respective mid-planes are visualized as orange dashed lines. Furthermore, a global reference plane with global coordinates is introduced (yellow dashed line). No requirements regarding the geometry of the adherends are made. The adherend thicknesses t_U and t_L may be different, just like the lengths of each section l_U , l_O , and l_L .

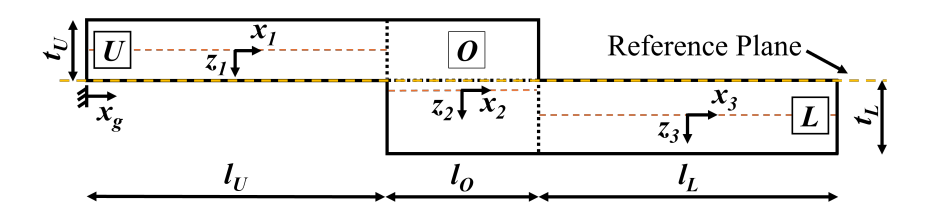


Fig. 2 Geometry and coordinate systems for the global single-lap shear joint analysis.

A. Kinematics

Each region of the SLS joint in Fig. 2 is described with the same kinematics. It is assumed that the joint is in cylindrical bending along the *x*-axis which implies that the structure is sufficiently wide and that its response is independent of the *y*-coordinate. Note that cylindrical bending prohibits bending deformations through the *xz*-plane. The through-the-thickness response is linearized so that each region can be represented by its mid-plane. A suitable displacement field is therefore given by Eq. (1) which is essentially first-order shear deformation theory for the cylindrical bending of plates.

$$u(x,z) = u_0(x) + z\Psi(x)$$

$$v(x) = v_0(x)$$

$$w(x) = w_0(x)$$
(1)

The displacements u, v, and w act along the coordinate axes x, y, and z. They consist of the mid-plane displacements u_0 , v_0 , and w_0 , as well as of the rotation of the mid-plane normal about the y-axis Ψ .

If small displacements and rotations are assumed, then the linear strain tensor components ε_{ij} are given by

$$\varepsilon_{xx} = \frac{du_0}{dx} + z \frac{d\Psi}{dx} = \varepsilon_{xx}^{(0)} + z\kappa_{xx}$$

$$\varepsilon_{xz} = \frac{1}{2} \left(\Psi + \frac{dw_0}{dx} \right) = \varepsilon_{xz}^{(0)}$$

$$\varepsilon_{xy} = \frac{1}{2} \frac{dv_0}{dx} = \varepsilon_{xy}^{(0)}$$
(2)

where $\varepsilon_{ij}^{(0)}$ are the mid-plane strains and κ_{ij} denotes the curvature term. All strain components other than ε_{xz} , ε_{xx} , and ε_{zz} are zero. This implies a state of plane strain which is consistent with the assumption of cylindrical bending.

B. Constitutive Equations

Each composite ply is assumed to follow orthotropic material behavior. Since three strain tensor components are zero ($\varepsilon_{yy} = \varepsilon_{zz} = \varepsilon_{yz} = 0$), the size of the stiffness matrix C must be reduced from 6x6 to 3x3. This is achieved by first rotating the compliance matrix in the local ply coordinate system \overline{S} to the global mid-plane coordinate system using

$$S = R\overline{S}R^{\mathrm{T}} \tag{3}$$

where S is the rotated compliance matrix, R is the corresponding rotation matrix, and the superscript T denotes a transpose.

Next, the equations for ε_{yy} , ε_{zz} , and ε_{yz} in the constitutive law for a single ply

$$\begin{cases}
\varepsilon_{xx} \\
\varepsilon_{yy} \\
\varepsilon_{zz} \\
2\varepsilon_{yz} \\
2\varepsilon_{xy}
\end{cases} = \begin{bmatrix}
S_{11} & S_{12} & S_{13} & 0 & 0 & S_{16} \\
S_{12} & S_{22} & S_{23} & 0 & 0 & S_{26} \\
S_{13} & S_{23} & S_{33} & 0 & 0 & S_{36} \\
0 & 0 & 0 & S_{44} & S_{45} & 0 \\
0 & 0 & 0 & S_{45} & S_{55} & 0 \\
S_{16} & S_{26} & S_{36} & 0 & 0 & S_{66}
\end{bmatrix} \begin{pmatrix}
\tau_{xx} \\
\tau_{yy} \\
\tau_{zz} \\
\tau_{yz} \\
\tau_{xz} \\
\tau_{xy}
\end{cases}$$
(4)

are set equal to zero to obtain expressions for the stresses τ_{yy} , τ_{zz} , and τ_{yz} . Then the corresponding terms in ε_{xx} , ε_{xz} , and ε_{xy} are eliminated. Since Eq. (4) allows for any rotation about the z-axis, layups in the analysis are not restricted to cross-ply laminates. Finally, the reduced compliance matrix is inverted to obtain

where the plane strain ply stiffness matrix entries Q_{ij} are not the same as in the classical laminated plate theory (CLPT).

C. Equilibrium Equations

The equilibrium equations are derived by setting the first variation of the total potential energy of each joint region equal to zero. The mathematics of the procedure are not shown here, but can be found in, for example, [14].

If the stress resultants N_{xx} , N_{xy} , Q_x , and M_{xx} are defined as

$$N_{xx} = \int_{-t/2}^{t/2} \tau_{xx} \, dz$$

$$N_{xy} = \int_{-t/2}^{t/2} \tau_{xy} \, dz$$

$$Q_x = \int_{-t/2}^{t/2} \tau_{xz} \, dz$$

$$M_{xx} = \int_{-t/2}^{t/2} \tau_{xx} z \, dz$$
(6)

then the equilibrium equations become

$$\frac{dN_{xx}}{dx} = 0$$

$$\frac{dN_{xy}}{dx} = 0$$

$$\frac{dQ_x}{dx} = 0$$

$$\frac{dM_{xx}}{dx} - Q_x = 0$$
(7)

These are equal to the well-known plate equilibrium equations when $\partial/\partial y = 0$. They are identical in each region because all joint sections are idealized in the same way. This is possible because the overlap region is not cut along the interface between the adherends which would give rise to tractions that would need to be accounted for in the corresponding equilibrium equations. While cutting the overlap region theoretically allows for a more appropriate enforcement of the free edge boundary condition later in the analysis, the displacement field in Eq. (1) constrains potential solutions to the one presented on the following pages. Hence, the simplified treatment of the overlap region is acceptable in the context of Eq. (1).

The relations between the stress resultants and the strains are

$$N_{xx} = A_{11}\varepsilon_{xx}^{(0)} + A_{16}\varepsilon_{xy}^{(0)} + B_{11}\kappa_{xx}$$

$$N_{xy} = A_{16}\varepsilon_{xx}^{(0)} + A_{66}\varepsilon_{xy}^{(0)} + B_{16}\kappa_{xx}$$

$$M_{xx} = B_{11}\varepsilon_{xx}^{(0)} + B_{16}\varepsilon_{xy}^{(0)} + D_{11}\kappa_{xx}$$

$$Q_{x} = kA_{55}\varepsilon_{xz}^{(0)}$$
(8)

where k is the shear correction factor. For simplicity, a value of k = 5/6 is assumed during the analysis. The plate stiffnesses A_{ij} , B_{ij} , and D_{ij} are expressed as

$$(A_{ij}, B_{ij}, D_{ij}) = \int_{-t/2}^{t/2} Q_{ij} (1, z, z^2) dz \qquad (i, j = 1, 5, 6)$$
(9)

which are again not equal to the plate stiffnesses from CLPT because the Q_{ij} are different. Since the plate stiffnesses do not get updated during the analysis, the formulation in Eq. (7) implies a geometrically linear approach, i.e., the equilibrium equations are satisfied on the undeformed structure.

D. General Solution

The general solution to the set of coupled ordinary differential equations (ODEs) is determined in each region by substituting Eqs. (8) and (2) into Eq. (7). Solutions for the displacement degrees of freedom are assumed in the form of exponential functions such that

$$(u_0, v_0, w_0, \Psi) = (C_1, C_2, C_3, C_4) e^{\lambda x}$$
(10)

This leads to the eigenvalue problem

$$\begin{bmatrix} A_{11}\lambda^2 & A_{16}\lambda^2 & 0 & B_{11}\lambda^2 \\ A_{16}\lambda^2 & A_{66}\lambda^2 & 0 & B_{16}\lambda^2 \\ 0 & 0 & kA_{55}\lambda^2 & kA_{55}\lambda \\ B_{11}\lambda^2 & B_{16}\lambda^2 & -kA_{55}\lambda & D_{11}\lambda^2 - kA_{55} \end{bmatrix} \begin{pmatrix} C_1 \\ C_2 \\ C_3 \\ C_4 \end{pmatrix} = \mathbf{0}$$

$$(11)$$

where nontrivial solutions only exist when the determinant of the coefficient matrix is zero. The characteristic equation

$$kA_{55} \left[\left(A_{11}A_{66} - A_{16}^2 \right) D_{11} - A_{11}B_{16}^2 + 2A_{16}B_{11}B_{16} - A_{66}B_{11}^2 \right] \lambda^8 = 0$$
 (12)

is easily solved for the eight eigenvalues λ which are all identically zero. Substitution into Eq. (10) immediately yields a constant as one of the solutions to the set of ODEs. The remaining seven linearly independent solutions are constructed as polynomials. Consequently, the displacement degrees of freedom may be written as

$$u_0, v_0, w_0, \Psi = \sum_{i=0}^{n=7} c_{ij} x^j$$
 $(i = 1, 2, 3, 4)$ (13)

where c_{ij} are yet undetermined coefficients.

When Eq. (13) is substituted back into Eq. (7), each equation must hold for any value of x. This yields additional constraints which relate different c_{ij} . Since not all additional equations are linearly independent, eight arbitrary c_{ij} remain as unknowns. These must be determined from the boundary conditions. Finally, the general solution is given by

$$u_{0} = c_{10} + c_{11}x - \frac{3(A_{16}B_{16} - A_{66}B_{11})}{A_{11}A_{66} - A_{16}^{2}}c_{33}x^{2}$$

$$v_{0} = c_{20} + c_{21}x + \frac{3(A_{11}B_{16} - A_{16}B_{11})}{A_{11}A_{66} - A_{16}^{2}}c_{33}x^{2}$$

$$w_{0} = c_{30} + \left\{ \frac{6\left[\left(B_{16}^{2} - A_{11}D_{11}\right)A_{11} + A_{16}^{2}D_{11} - 2A_{16}B_{11}B_{16} + A_{66}B_{11}^{2}\right]}{kA_{55}\left(A_{11}A_{66} - A_{16}^{2}\right)}c_{33} - c_{40} \right\}x + c_{32}x^{2} + c_{33}x^{3}$$

$$\Psi = c_{40} - 2c_{32}x - 3c_{33}x^{2}$$

$$(14)$$

Eq. (14) is only valid as the solution to the set of ODEs in Eq. (7) when all coupling terms in Eq. (8) are present. If a laminate is symmetric ($B_{ij} = 0$), then the out-of-plane response decouples from the in-plane response. If the same laminate is furthermore balanced ($A_{16} = 0$), then the solution in the y-direction also decouples from the solution in the directions of x and z.

E. Single-Lap Shear Joint Solution

The general solution in Eq. (14) is applicable to every region in Figure 2. Hence, the individual solutions must be related to each other such that they represent the entire SLS joint. This is achieved by considering various boundary and continuity conditions. Before these conditions are formulated, it is important to specify the same reference plane for all variables and quantities. Therefore, the plate stiffnesses computed in Eq. (9) are adjusted to the location of the reference plane in Figure 2. The new, offset values are given by

$$A^{\text{off}} = A$$

$$B^{\text{off}} = B + d_i A$$

$$D^{\text{off}} = D + 2d_i B + d_i^2 A$$
(15)

where d_i are the distances from each region's mid-plane to the reference plane, i.e.,

$$d_U = \frac{t_U}{2} \qquad d_L = -\frac{t_L}{2} \qquad d_O = \frac{t_U - t_L}{2} \tag{16}$$

Because of the shift, all section coordinate systems move onto the reference plane. Consequently, the final results for the displacement degrees of freedom are expressed with respect to this plane. The ranges for the through-the-thickness coordinates become

$$U: -t_U \le z_1 \le 0 \qquad O: -t_U \le z_2 \le t_L \qquad L: 0 \le z_3 \le t_L \tag{17}$$

Four boundary conditions must be prescribed at the end of each region. Considering the load case in Fig. 1, a displacement load u_{init} is applied on the left side of the joint. Assuming that all other displacement degrees of freedom are restricted, the first four boundary conditions for the upper adherend are

$$u_{0II}(x_1 = -l_{II}/2) = -u_{init} (18a)$$

$$v_{0U}(x_1 = -l_U/2) = 0 (18b)$$

$$w_{0U}(x_1 = -l_U/2) = 0 (18c)$$

$$\Psi_U(x_1 = -l_U/2) = 0 \tag{18d}$$

where the subscript U is introduced to denote the upper adherend. Similarly, the subscripts O and L are used for the overlap region and the lower adherend, respectively.

The lower adherend is clamped at its right end. Therefore,

$$u_{0L}(x_3 = l_L/2) = 0 (19a)$$

$$v_{0L}(x_3 = l_L/2) = 0 (19b)$$

$$w_{0L}(x_3 = l_L/2) = 0 (19c)$$

$$\Psi_L(x_3 = l_L/2) = 0 (19d)$$

The remaining 16 boundary conditions prescribe the displacement and stress resultant continuity at the junctions between the two adherends and the overlap region. At the connection between the upper adherend and the overlap region, they are

$$u_{0U}(x_1 = l_U/2) = u_{0O}(x_2 = -l_O/2)$$
 (20a)

$$v_{0U}(x_1 = l_U/2) = v_{0O}(x_2 = -l_O/2)$$
 (20b)

$$w_{0U}(x_1 = l_U/2) = w_{0O}(x_2 = -l_O/2)$$
(20c)

$$\Psi_U(x_1 = l_U/2) = \Psi_O(x_2 = -l_O/2) \tag{20d}$$

$$N_{xxU}(x_1 = l_U/2) = N_{xxO}(x_2 = -l_O/2)$$
 (20e)

$$N_{xyU}(x_1 = l_U/2) = N_{xyO}(x_2 = -l_O/2)$$
(20f)

$$M_{xxU}(x_1 = l_U/2) = M_{xxO}(x_2 = -l_O/2)$$
 (20g)

$$Q_{xU}(x_1 = l_U/2) = Q_{xO}(x_2 = -l_O/2)$$
 (20h)

and at the connection between the overlap region and the lower adherend the relations

$$u_{0O}(x_2 = l_O/2) = u_{0L}(x_3 = -l_L/2)$$
 (21a)

$$v_{0O}(x_2 = l_O/2) = v_{0L}(x_3 = -l_L/2)$$
 (21b)

$$w_{0O}(x_2 = l_O/2) = w_{0L}(x_3 = -l_L/2)$$
 (21c)

$$\Psi_O(x_2 = l_O/2) = \Psi_L(x_3 = -l_L/2) \tag{21d}$$

$$N_{xxO}(x_2 = l_O/2) = N_{xxL}(x_3 = -l_L/2)$$
 (21e)

$$N_{xyO}(x_2 = l_O/2) = N_{xyL}(x_3 = -l_L/2)$$
 (21f)

$$M_{xxO}(x_2 = l_O/2) = M_{xxL}(x_3 = -l_L/2)$$
 (21g)

$$Q_{xO}(x_2 = l_O/2) = Q_{xL}(x_3 = -l_L/2)$$
 (21h)

are imposed.

The stress resultant continuity conditions in Eqs. (20e) to (20h) and Eqs. (21e) to (21h) introduce an error because they neglect the free edge boundary conditions at the two overlap ends. The equations immediately smear the stress resultants from each adherend over the entire thickness of the overlap region instead of only over the corresponding cross-sections of the upper and lower adherend. Anyhow, the above constraints lead to a linear system of 24 equations for 24 unknown c_{ij} . While a closed-form solution is possible, it is considerably more convenient to substitute values for all geometric and stiffness parameters to determine numerical values of c_{ij} . Once the c_{ij} are known, substituting them into Eq. (14) yields the final solution from which all other quantities can be calculated using Eqs. (1), (2), and (8).

IV. Finite Element Models

2D and 3D finite element (FE) models are created in Abaqus 2023 for the verification of the analytical solution. The analyses are static and linear like the solution developed in Section III. The only deviation is made when additional simulations are run to check the effect of accounting for large deformations on the predictions. The composite material considered is unidirectional Toray Cetex[®] TC1225 LMPAEK[™] [16] which consists of T700 fibers embedded in a low-melt polyaryletherketone matrix (T700/LM-PAEK). Each ply is assumed to be transversely isotropic. The corresponding material properties are listed in Table 1.

Table 1 Elastic properties of T700/LM-PAEK [17, 18].

Young's modulus in 1-direction E_1	130.5 GPa
Young's modulus in 2-direction E_2	9.087 GPa
Shear modulus in 12-direction G_{12}	4.646 GPa
Poisson's ratio in 12-direction v_{12}	0.3371
Poisson's ratio in 23-direction v_{23}	0.48

To showcase the applicability of the analytical solution to welded thermoplastic composite SLS joints with arbitrary layups and laminate thicknesses, different layups for each adherend are modeled (Table 2). These layups are chosen because they feature all coupling terms that are part of Eq. (8).

Table 2 Composite layups in the adherends.

Upper adherend	[45,0,45,90,0,45,90,-45,-45,90,45,0]
Lower adherend	$[0,\!45,\!90,\!-45,\!90,\!45,\!-45,\!0,\!45,\!0,\!45,\!90,\!90,\!45,\!0,\!-45]$

All simulations are repeated for aluminum 2024-T3 with the elastic properties reported in Table 3 which allows benchmarking the composite predictions in 2D and 3D with the isotropic case.

Table 3 Elastic properties of aluminum 2024-T3.

Young's modulus E	73.1 GPa
Poisson's ratio ν	0.33

The dimensions of the SLS joint are summarized in Table 4. They follow the specimen geometry described in the test standard ASTM D5868 [19]. The laminate thicknesses are the result of a constant ply thickness of 0.1325 mm. For the 3D case, each joint is considered to be 25.4 mm wide in accordance with ASTM D5868.

Table 4 Dimensions of the single-lap shear joint.

t_U	t_L	l_U	l_O	l_L
1.65 mm	2.2 mm	76.2 mm	25.4 mm	76.2 mm

A. 2D Model

The 2D model is shown in Fig. 3. It uses 14224 CPE4I elements that are connected at 15270 nodes with a mesh size of approximately 0.2 mm. CEP4I is a plane strain element with incompatible modes for an improved bending response. The boundary conditions match those sketched in Fig. 1, i.e., a uniform axial displacement load of 0.4 mm is applied on the left joint end and the right end is clamped.



Fig. 3 Overview of the 2D single-lap shear joint model.

Each ply in the joint is modeled separately. Since Abaqus only permits composite layup rotations about the normal to the modeling plane, it is not possible to use the built-in modules to generate ply rotations other than 0° or 90° . Hence, the ply stiffnesses are computed externally by inverting the result of Eq. (3) and then assigning them to an anisotropic homogeneous solid section. Consequently, one material must be defined per ply orientation which is subsequently applied to the individual plies according to the laminate layup.

The interface between the upper and lower adherend is idealized as a cohesive surface without damage. The stiffness of the corresponding traction-separation curve is determined by the solver.

B. 3D Model

SC8R reduced integration continuum shell elements are used to discretize the 3D model. They only feature translational degrees of freedom, so it is sufficient to prescribe these quantities on the joint ends as shown in Fig. 4 to simulate the boundary conditions from Fig. 1. To evaluate the effect of plane strain in a 3D model, two different cases are studied: one where the lateral edges of the joint are allowed to freely deform, and one where the boundary condition U2 = 0 is applied to simulate plane strain in 3D.

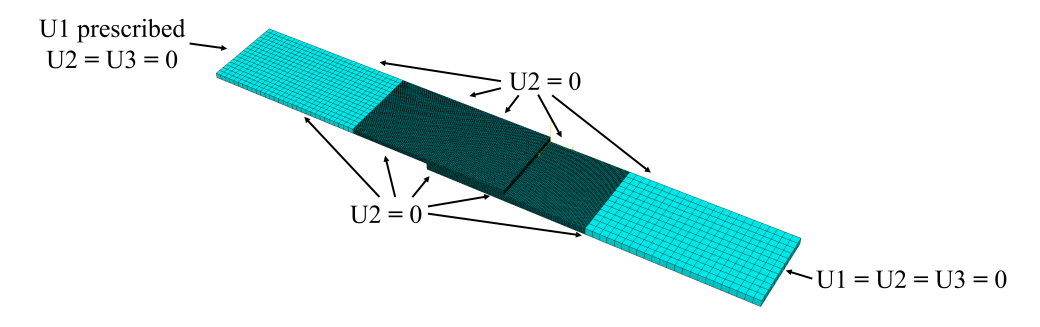


Fig. 4 Mesh and boundary conditions of the 3D single-lap shear joint model. Lateral constraints (U2 = 0) are only active when simulating plane strain in 3D.

A mesh with one element through the thickness is used in the outer regions. In the center, two plies are represented by one continuum shell element. This results in around 454000 elements and 525000 nodes. The outer sections are connected to the overlap region via tie constraints. Rotations of individual plies are specified in the composite layup module. Again, the interface between the two adherends is modeled as a cohesive surface without damage where the stiffness of the traction-separation law is determined by the solver.

V. Results

A. Comparison of Finite Element Models

Evaluating the results of the various FE simulations aids in determining which assumptions in the analytical model have a relevant influence on the predictions. Two outputs are tracked for this purpose. The first one is the maximum out-of-plane displacement U3 of the joint which relates to the amount of bending in the structure. The second one is the sum of the axial reaction forces RF1 at the clamped joint end. Since a known displacement load is applied, RF1 varies with the axial stiffness of the joint.

First, the influence of the different modeling choices on the numerical predictions is determined. Table 5 summarizes the two tracked outputs for the isotropic case which precludes potential errors originating from assigning the rotated ply stiffnesses differently in 2D and 3D. Looking at the first set of values for the geometrically linear case, it can be seen that switching from 2D to 3D considerably affects the joint stiffness. This is caused by the relatively small width of the structure which suggests that the assumption of plane strain is not necessarily justified. As a consequence, RF1 is overpredicted by approximately 10% in 2D compared to 3D. Restricting the lateral deflection on the sides of the joint as shown in Fig. 4 to simulate plane strain in the 3D model compensates for this effect almost entirely.

While the same trends are also observed for the geometrically nonlinear simulations, the absolute values of the predictions differ significantly, e.g., the maximum out-of-plane displacement U3 in 3D is 2.583 mm in the linear analysis compared to 0.583 mm for the nonlinear case. SLS joints exhibit secondary bending due to their geometry even when

only in-plane loads are applied. The bending leads to the rotation of the overlap region into the load path which increases its apparent axial stiffness and reduces the out-of-plane deformation because a larger portion of the structure is loaded in a membrane state of stress. Considering that the prescribed displacement load of 0.4 mm causes an average axial strain of 0.225%, it becomes clear that satisfying the equilibrium equations on the deformed structure in the geometrically nonlinear analysis is the main source of the deviation.

Table 5 FE benchmark results for aluminum 2024-T3.

geometrically linear						geom	etrically no	onlinear		
	2D	3D	Change	3D*	Change	2D	3D	Change	3D*	Change
Max U3 [mm]	2.601	2.583	-0.7%	2.613	0.5%	0.576	0.583	1.2%	0.579	0.5%
RF1 [kN]	6.38	5.8	-9.1%	6.39	0.2%	8.54	7.68	-10.1%	8.56	0.3%

^{*} Model that simulates the plane strain condition in 3D by restricting the lateral deformation on the sides of the joint.

The benchmark results for the composite laminate are listed in Table 6 and include the effects of assigning the rotated ply stiffnesses in 2D as an anisotropic homogeneous solid section. It is evident that even though simulating the plane strain condition in 3D reduces the difference between the predictions of the 2D and 3D models, they do not reach the same level of agreement as for the isotropic reference case. Nevertheless, they are reasonably close. The remaining discrepancy is caused by the anisotropy of the composite layup. Stresses and strains vary significantly along the width of each ply and trying to capture this behavior at a single point along the cross-section, as implicitly assumed by the 2D model, necessarily introduces an error. Hence, the 2D model is considered to be sufficiently accurate if the assumption of plane strain is satisfied.

Table 6 FE benchmark results for T700/LM-PAEK.

	geometrically linear						geom	etrically no	onlinear	
	2D	3D	Change	3D*	Change	2D	3D	Change	3D*	Change
Max U3 [mm]	2.15	2.307	7.5%	2.241	4.2%	0.542	0.651	20.2%	0.561	3.6%
RF1 [kN]	4.52	3.99	-11.9%	4.35	-3.9%	5.78	5.12	-11.5%	5.61	-3.1%

^{*} Model that simulates the plane strain condition in 3D by restricting the lateral deformation on the sides of the joint.

B. Verification of Analytical Model

The predictions of the analytical model are verified with geometrically linear FE simulations. Material properties, composite layup, and joint dimensions are taken from Tables 1, 2, and 4. The applied displacement load is equal to the displacement prescribed in the numerical models, i.e., $u_{init} = 0.4$ mm. Since the analytical model makes some simplifying assumptions at the overlap ends, the axial and out-of-plane reference plane deformations along the joint length are compared to the numerical predictions. These quantities are relative to the reference plane shown in Fig. 2. The corresponding numerical values are sampled at the equivalent position in the FE models. For the 3D case, the mid-span across the joint width is considered.

Figure 5 plots the analytical prediction for the axial reference plane displacement u_0 against the numerical results. While the overall agreement is excellent, small deviations are observed close to the ends of the overlap region which extends from $x_g = 76.2$ mm to $x_g = 101.6$ mm.

Similarly, the out-of-plane deformation w_0 is shown in Figure 6 as a function of the global x-coordinate. Again, the analytical prediction is very close to the numerical results. Here, variations are visible further away from the overlap region compared to Fig. 5. The maximum out-of-plane deformation values do not necessarily occur at the same location.

The discrepancy between the analytical prediction and the numerical simulations is the result of not exactly accounting for the free edge boundary conditions at the overlap ends. While the stress resultant continuity is prescribed in Eqs. (20e) to (20h) and Eqs. (21e) to (21h), the local stress distribution that is the result of these constraints is sketched in Fig. 7a. On average, i.e., when integrating the stresses over the entire thickness of the overlap region, the conditions imposed in the aforementioned equations are equivalent to the correct free edge boundary condition depicted

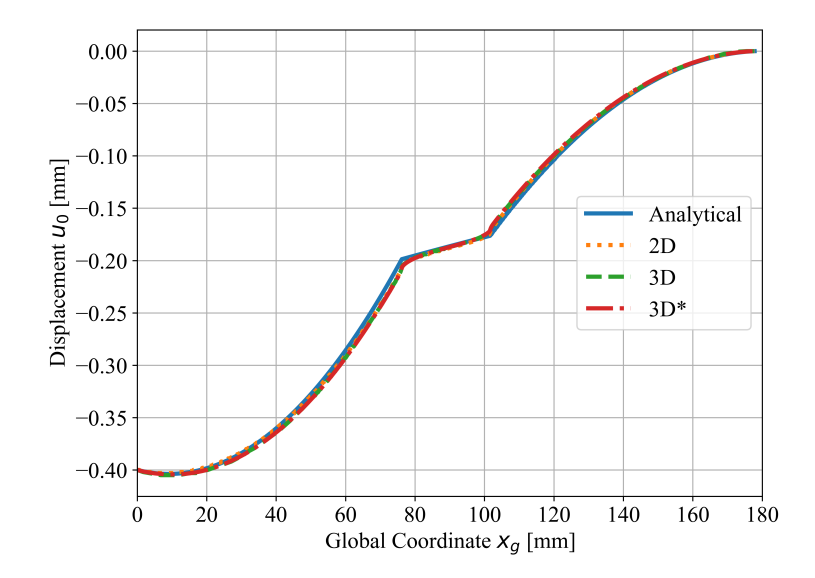


Fig. 5 Axial reference plane deformation along the joint length. * denotes plane strain simulated in a 3D model.

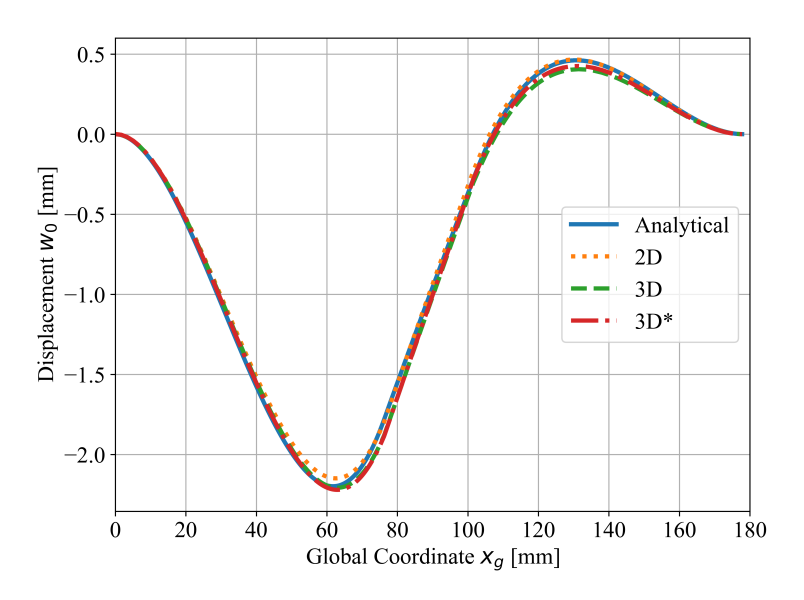
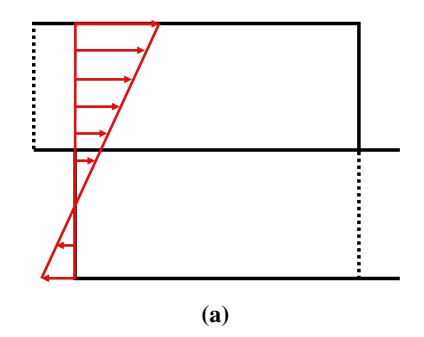


Fig. 6 Out-of-plane deformation along the joint length. * denotes plane strain simulated in a 3D model.

in Fig. 7b. However, the free edge boundary conditions are not correct locally and therefore the corresponding stress distribution is oversimplified. This is the inconsistency that Hart-Smith [4] alleges to have determined in the adhesively bonded SLS joint analysis of Goland and Reissner [3]. The stress resultants from each adherend are immediately smeared over the entire thickness of the overlap region instead of only being transferred to the relevant adherend cross-section. Consequently, the present analysis overestimates the stiffness of the overlap region compared to the numerical models. The discrepancies outside of the joint region are a mathematical consequence of this effect.

Since the entire displacement field is known from the analysis, it is also possible to compare the stress resultants with the reaction forces from the FE simulations. All analytical stress resultants except for the bending moment, which varies linearly, are constant because of the simplicity of the model. The analytical values are converted to the forces in Table 7 by multiplying them by the 3D joint width of 25.4 mm. The reaction forces at the clamped end in the analytical model are 8% (RF1) and 7% (RF2) higher than the predictions in the 2D FE models due to the overestimation of the stiffness in the overlap region.



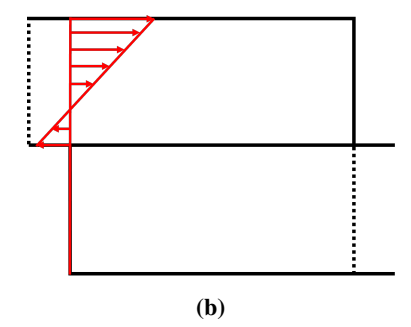


Fig. 7 Sketch of the stress distribution at one overlap end (a) as assumed in the present analysis and (b) when correctly accounting for the stress-free condition at the free edge.

Table 7 Stress resultants at the clamped end.

	Analytical	2D	3D	3D*
RF1 [kN]	4.87	4.52	3.99	4.35
RF2 [N]	-75.0	-69.9	-62.3	-67.6

^{*} Plane strain simulated in 3D.

Even though the accuracy of the stress resultants is not as good as the estimation of the displacement degrees of freedom, the verification of the analytical model with the FE simulations shows that the global structural response is captured well when the underlying assumptions are satisfied. Hence, the analytical model is suitable for providing input for more detailed analyses, e.g., for determining the interlaminar stress distribution at the welded interface between the two adherends.

VI. Conclusion

A simple analytical model for predicting the structural response of composite single-lap shear joints is developed and verified with numerical simulations of welded thermoplastic composite specimens. The two-dimensional model does not place any restrictions on the composite layup or on the dimensions of the adherends and closely matches the displacement field of the numerical simulations if the underlying assumptions of small deformations and plane strain are fulfilled. Small deviations in the displacement field predictions are observed close to the overlap region because the stress-free boundary condition at the overlap ends is only satisfied in an average sense. As a result, the joint stiffness is overestimated which leads to an overprediction of the forces in the joint compared to the numerical simulations. Nevertheless, the analytical model is a suitable tool to provide input for more detailed single-lap shear joint analyses, for example for the determination of the interlaminar stresses at the interface between the two adherends.

References

- [1] De Jong, T., "On the Calculation of Stresses in Pin-loaded Anisotropic Plates," Ph.D. thesis, Delft University of Technology, 1989.
- [2] Koord, J., Stüven, J.-L., Völkerink, O., Petersen, E., and Hühne, C., "Investigation of Exact Analytical Solutions for Composite Laminates under Pin-bearing Loading," *Composite Structures*, Vol. 292, 2022, p. 115605. https://doi.org/10.1016/j.compstruct. 2022.115605.
- [3] Goland, M., and Reissner, E., "The Stresses in Cemented Joints," *Journal of Applied Mechanics*, Vol. 11, No. 1, 1944, pp. A17–A27. https://doi.org/10.1115/1.4009336.
- [4] Hart-Smith, L. J., Adhesive-Bonded Single-Lap Joints, NASA CR-112236, 1973.
- [5] Yang, C., and Pang, S.-S., "Stress-strain Analysis of Single-lap Composite Joints under Tension," *Journal of Engineering Materials and Technology*, Vol. 1182, No. 2, 1996, pp. 247–255. https://doi.org/10.1115/1.2804896.

- [6] Zhang, J., Bednarcyk, B., Collier, C., Yarrington, P., Bansal, Y., and Pindera, M.-J., "3D Stress Analysis of Adhesively Bonded Composite Joints," 46th AIAA/ASME/ASCE/AHS/ASC Structures, Structural Dynamics and Materials Conference, Austin, Texas, 2005, p. 2021. https://doi.org/10.2514/6.2005-2021.
- [7] Tijs, B. H. A. H., Abdel-Monsef, S., Renart, J., Turon, A., and Bisagni, C., "Characterization and Analysis of the Interlaminar Behavior of Thermoplastic Composites considering Fiber Bridging and R-curve Effects," *Composites Part A: Applied Science and Manufacturing*, Vol. 162, 2022, p. 107101. https://doi.org/10.1016/j.compositesa.2022.107101.
- [8] Ageorges, C., Ye, L., and Hou, M., "Advances in Fusion Bonding Techniques for Joining Thermoplastic Matrix Composites: A Review," Composites Part A: Applied Science and Manufacturing, Vol. 32, No. 6, 2001, pp. 839–857. https://doi.org/10.1016/ S1359-835X(00)00166-4.
- [9] Pipes, R. B., and Pagano, N. J., "Interlaminar Stresses in Composite Laminates under Uniform Axial Extension," *Journal of Composite Materials*, Vol. 4, No. 4, 1970, pp. 538–548. https://doi.org/10.1177/002199837000400409.
- [10] Kant, T., and Swaminathan, K., "Estimation of Transverse/Interlaminar Stresses in Laminated Composites A Selective Review and Survey of Current Developments," *Composite Structures*, Vol. 49, 2000, pp. 65–75. https://doi.org/10.1016/S0263-8223(99)00126-9.
- [11] Mittelstedt, C., Becker, W., Kappel, A., and Kharghani, N., "Free-edge Effects in Composite Laminates A Review of Recent Developments 2005–2020," *Applied Mechanics Reviews*, Vol. 74, 2022, p. 10801. https://doi.org/10.1115/1.4054145.
- [12] Wang, S., and Choi, I., "Boundary-layer Effects in Composite Laminates: Part 2 Free-edge Stress Solutions and Basic Characteristics," *Journal of Applied Mechanics*, Vol. 49, No. 3, 1982, pp. 549–560. https://doi.org/10.1115/1.3162521.
- [13] Lekhnitskii, S. G., Theory of Elasticity of an Anisotropic Elastic Body, Mir Publishers, Moscow, 1981.
- [14] Reddy, J. N. (ed.), Mechanics of Composite Materials: Selected Works of Nicholas J. Pagano, Springer Science & Business Media, Dordrecht, 1994.
- [15] Kassapoglou, C., and DiNicola, A. J., "Efficient Stress Solutions at Skin Stiffener Interfaces of Composite Stiffened Panels," AIAA Journal, Vol. 30, No. 7, 1992, pp. 1833–1839. https://doi.org/10.2514/3.11144.
- [16] Toray Advanced Composites, Toray Cetex® TC1225 LMPAEK™ Product Data Sheet, 2023.
- [17] Lian, E., Medium Toughness PAEK Thermoplastics Toray Cetex® TC1225 (LM PAEK) T700GC 12K T1E Unidirectional Tape 145 gsm 34% RC Qualification Material Property Data Report, CAM-RP-2019-036 Rev A, 2021.
- [18] Tijs, B. H. A. H., Doldersum, M. H. J., Turon, A., Waleson, J. E. A., and Bisagni, C., "Experimental and Numerical Evaluation of Conduction Welded Thermoplastic Composite Joints," *Composite Structures*, Vol. 281, 2022, p. 114964. https://doi.org/10.1016/j.compstruct.2021.114964.
- [19] ASTM International, ASTM D5868-01: Standard Test Method for Lap Shear Adhesion for Fiber Reinforced Plastic (FRP) Bonding, 2023.